11-2001

Taylor Cone and Jetting from Liquid Droplets in Electrospinning of Nanofibers

Alexander L. Yarin

S Koombhongse

Darrell Hyson Reneker
University of Akron Main Campus, reneker@uakron.edu

Taylor cone and jetting from liquid droplets in electrospinning of nanofibers

A. L. Yarin
Faculty of Mechanical Engineering, Technion, Haifa 32000, Israel

S. Koombhongse and D. H. Reneker[a)]
Maurice Morton Institute of Polymer Science, Department of Polymer Science, The University of Akron, Akron, Ohio 44325-3909

(Received 7 September 2000; accepted for publication 10 August 2001)

Sessile and pendant droplets of polymer solutions acquire stable shapes when they are electrically charged by applying an electrical potential difference between the droplet and a flat plate, if the potential is not too large. These stable shapes result only from equilibrium of the electric forces and surface tension in the cases of inviscid, Newtonian, and viscoelastic liquids. In liquids with a nonrelaxing elastic force, that force also affects the shapes. It is widely assumed that when the critical potential φ_{0*} has been reached and any further increase will destroy the equilibrium, the liquid body acquires a conical shape referred to as the Taylor cone, having a half angle of 49.3°. In the present work we show that the Taylor cone corresponds essentially to a specific self-similar solution, whereas there exist nonself-similar solutions which do not tend toward a Taylor cone. Thus, the Taylor cone does not represent a unique critical shape: there exists another shape, which is not self-similar. The experiments of the present work demonstrate that the observed half angles are much closer to the new shape. In this article a theory of stable shapes of droplets affected by an electric field is proposed and compared with data acquired in our experimental work on electrospinning of nanofibers from polymer solutions and melts. © *2001 American Institute of Physics.* [DOI: 10.1063/1.1408260]

I. INTRODUCTION

Rayleigh[1] studied theoretically the stability of an isolated charged liquid droplet and predicted that it becomes unstable and fission takes place when the charge becomes sufficiently large compared to the stabilizing effect of the surface tension. Zeleny[2] tried to adapt this theory to the case of an electrified droplet losing its stability when jetting begins at its vertex. His theoretical results were corrected by Taylor[3] in seminal work in which the spheroidal approximation of droplet shapes was proposed for the case of (i) a charged droplet sustained at a given potential Φ_0 relative to the ground, or (ii) an uncharged droplet in a given uniform field E.

Taylor showed that in case (i) a droplet raised to a potential Φ_0 could be sustained by surface tension in equilibrium with its own electric field provided the Rayleigh condition was satisfied, namely, at $\Phi_0(\pi R_0\sigma)^{-1/2}<4$, where R_0 is the volume-equivalent droplet radius, and σ is the surface tension coefficient. In spite of the fact that case (i) is quite similar to the situation in which a droplet is attached to an electrode mounted at some potential Φ_0 relative to the ground, the predictions of the spheroidal approximation do not agree with the experimental evidence. Instead, the theory predicted that, as Φ_0 increases and approaches the critical (Rayleigh) value, the stable shape becomes less and less prolate, tending toward a sphere, whereas in the experiment an increase in the potential results in more prolate droplets.

Case (ii) corresponds to a droplet positioned inside a capacitor. As the strength of the field E increases, the droplet becomes more and more prolate until no shape is stable beyond some critical value E^*. This resembles the behavior recorded in Ref. 3 for droplets subjected to a higher and higher potential Φ_0: they elongate to some extent, but then suddenly tend toward a cone-like shape. The boundary between the stable electrified droplets and those with a jet flowing from the tip lies somewhere near this potential. Taylor calculated the half angle at the tip of an infinite cone arising from an infinite liquid body. In Sec. II we calculate the half angle by a different method which brings out the self-similar nature of the Taylor cone, and state the assumptions involved in its calculation. Then, in Sec. III we consider a family of nonself-similar solutions for the hyperboloidal shapes of electrified liquid bodies in equilibrium with their own electric field due to surface tension forces. In Sec. IV we show that these solutions do not tend toward a self-similar solution corresponding to the family of the Taylor cone, and represent an alternative to the Taylor cone. Thus we conclude that another shape, one tending towards a sharper cone than that of Taylor, can precede the stability loss and the onset of jetting. In Sec. V we consider predictions of the hyperboloidal approximation in the case of bodies of elastic liquids. In Sec. VI experimental results are presented and compared with the theory. These results confirm the theoretical predictions of Sec. IV. A summary is presented in Sec. VII.

a)Electronic mail: dhr@polymer.uakron.edu

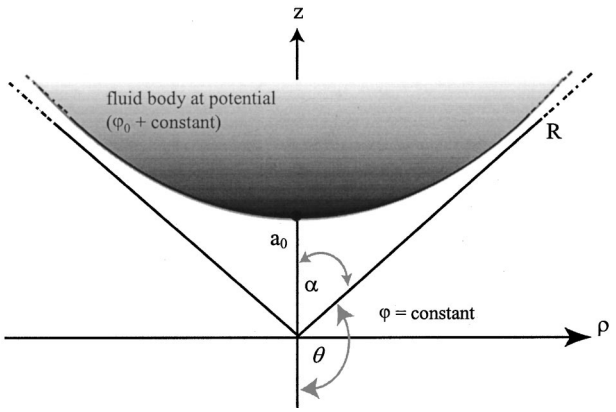

FIG. 1. Axisymmetric "infinite" fluid body kept at potential $\Phi_0=\varphi_0+\text{const}$ at a distance a_0 from an equipotential plane kept at $\Phi=\text{const}$.

II. TAYLOR CONE AS A SELF-SIMILAR SOLUTON

All the liquids we deal with throughout the article are ionic conductors. Under the influence of an applied potential difference, excess charge flows to or from the liquid. Anions and cations are distributed nonuniformly on the surface of the liquid. The free surfaces of the liquids are always equipotential surfaces with the charges distributed in a way that maintains a zero electric field inside the liquid.

To establish the self-similar nature of the solution corresponding to the Taylor cone, we consider an axisymmetric liquid body kept at a potential ($\varphi_0+\text{const}$) with its tip at a distance a_0 from an equipotential plane (Fig. 1). The distribution of the electric potential $\Phi=\varphi+\text{const}$ is described in the spherical coordinates R and θ, and in cylindrical coordinates ρ and z (see Fig. 1). The shape of the free surface is assumed to be that of equilibrium, which means that the electrical forces acting on the droplet in Fig. 1 are balanced by the surface tension forces. The potential φ_0 can, in such a case, always be expressed in terms of the surface tension coefficient σ and of a_0, specifically as $\varphi_0=C(\sigma a_0)^{1/2}$, where C is a dimensionless factor. Due to the dimensional arguments the general representation of φ is, in the present case, $\varphi=\varphi_0 F_1(R/a_0,\theta)$, where F_1 is a dimensionless function. The value of the potential Φ at any point throughout the space that surrounds the liquid body is given by

$$\Phi=(\sigma a_0)^{1/2}F\left(\frac{R}{a_0},\theta\right)+\text{const}, \tag{1}$$

where $F=CF_1$ is a dimensionless function.

At distances $R\gg a_0$, where it can be assumed that the influence of the gap a_0 is small, the function F should approach a specific power-law scaling,

$$F\left(\frac{R}{a_0},\theta\right)=\left(\frac{R}{a_0}\right)^{1/2}\Psi(\theta) \tag{2}$$

[$\Psi(\theta)$ being a dimensionless function], whereupon Eq. (1) takes the asymptotic self-similar form, independent of a_0,

$$\Phi=(\sigma R)^{1/2}\Psi(\theta)+\text{const}. \tag{3}$$

Power-law scalings leading to self-similar solutions are common in boundary-layer theory (cf., for example, Refs. 4 and 5, and references therein). In particular, such self-similar solutions, for jets and plumes considered as issuing from a pointlike source, in reality correspond to the nonself-similar solutions of the Prandtl equations for the jets and plumes being issued from finite-size nozzles, at distances much larger than the nozzle size.[5,6] The remote-asymptotic and self-similar solution[7] for capillary waves produced by weak impact of a droplet of diameter D onto a thin liquid layer, emerges at distances much greater than D from the center of impact. The self-similar solution for the electric field, Eq. (3), is motivated by precisely the same idea, and is expected to be the limit to all nonself-similar solutions at distances $R\gg a_0$.

This solution should also satisfy the Laplace equation, which enables us to find Ψ as[3]

$$\Psi(\theta)=P_{1/2}(\cos\theta), \tag{4}$$

where $P_{1/2}(\cos\theta)$ is a Legendre function of the order of 1/2.

The free surface becomes equipotential only when θ corresponds to the only zero of $P_{1/2}(\cos\theta)$ in the range of $0\geqslant\theta\leqslant\pi$, which is $\theta_0=130.7°$.[3] Then the fluid body shown in Fig. 1 is enveloped by a cone with the half angle at its tip equal to $\alpha=\alpha_T=\pi-\theta_0=49.3°$, which is the Taylor cone.[3] The shape of the liquid body in Fig. 1 would then approach the Taylor cone asymptotically as $R\to\infty$. Taylor's self-similarity assumption leading to Eqs. (2) and (3) also specifies that $\Phi\to\infty$ as $R\to\infty$, which is quite peculiar. In Sec. III we show that a relevant nonself-similar solution does not follow this trend $R\to\infty$, which means that these solutions are fundamentally different from the solution corresponding to the Taylor cone.

III. NONSELF-SIMILAR SOLUTIONS FOR HYPERBOLOIDAL LIQUID BODIES

Experimental data of Ref. 3 and numerous subsequent works show that droplets acquire a static shape that does not depend on the initial shape. This static shape is stable if the strength of the electric field does not exceed a certain critical level. As the electric field approaches the critical value, the droplet shape approaches that of a cone with a rounded tip. The radius of curvature of the tip can become too small to be seen in an ordinary photograph (to be discussed in Sec. VI). Nevertheless, the tip should be rounded, since otherwise the electric field would become infinite at the tip.[8] Detailed calculation of the exact droplet shape near the tip is an involved nonlinear integrodifferential problem, since the field depends on the droplet shape and vice versa. To simplify such calculations, approximate methods were proposed.[3,9,10] In those approximate methods a likely shape for a droplet is chosen that would satisfy the stress balance between the electric field and surface tension in an approximate way. In the present problem any likely droplet shape must be very close to a hyperboloid of revolution. Therefore the first theoretical assumption is that the droplet shape is a hyperboloid of revolution. In this article we show that such a hyperboloidal droplet approaches a static shape that is very close to that of a cone with a rounded tip. The tip has a very small radius of curvature. This hyperboloid corresponds to the experimental evidence (discussed in Sec. VI).

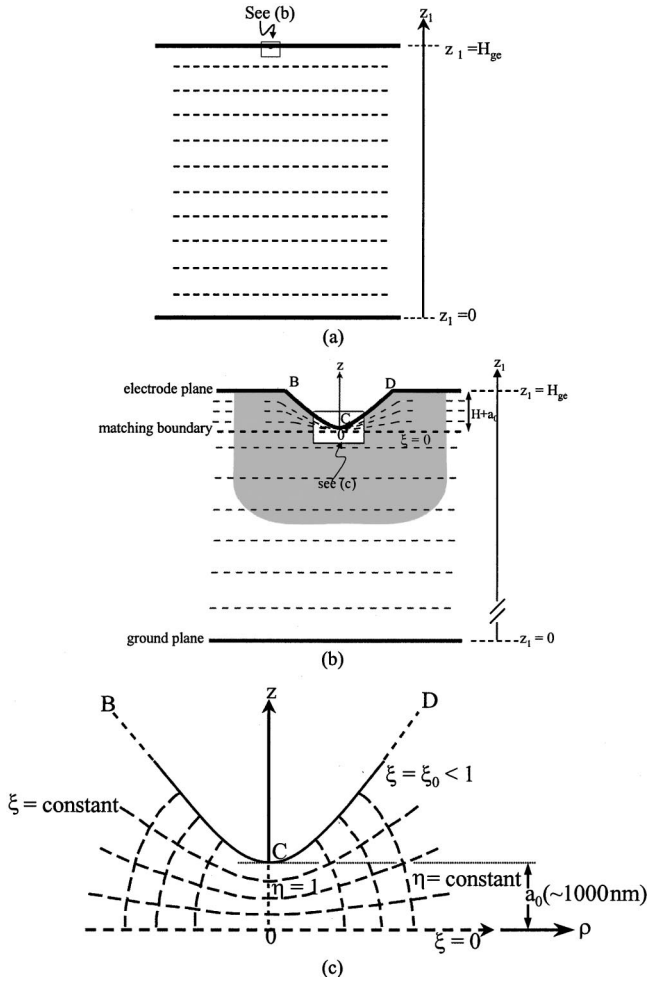

FIG. 2. Prolate spheroidal coordinate system about a hyperboloidal liquid body BCD. (a) Equipotential lines are shown for $0 \leqslant z_1 \leqslant H_{ge}-(H+a_0)$. (c) Equipotential lines ($\xi=$const) are shown for $H_{ge}-(H+a_0) \leqslant z_1 \leqslant H_{ge}$.

In calculating an electric field about a body shaped as a hyperboloid of revolution, like the one denoted BCD in Figs. 2(b) and 2(c), it is natural to use the prolate spheroidal coordinate system ξ, η. We assume that the tip of the hyperboloid BCD is situated at a distance a_0 from the equipotential surface $z=0$, and the range in which a solution is sought corresponds to $0 \leqslant \xi \leqslant \xi_0 < 1$, $1 \leqslant \eta \leqslant \infty$. The surface of hyperboloid BCD is represented by ξ_0 [see Fig. 2(c)]. Coordinate isolines are also shown in Fig. 2, with the lines $\eta=$const representing ellipsoids, and the lines $\xi=$const representing hyperboloids.

The second theoretical assumption is that the space charge effects are negligible. This assumption is discussed in detail in Sec. VI. Then the electric potential Φ satisfies the Laplace equation. In prolate spheroidal coordinates it takes the form,[11]

$$\frac{\partial}{\partial \xi}\left((1-\xi^2)\frac{\partial \Phi}{\partial \xi}\right)+\frac{\partial}{\partial \eta}\left((\eta^2-1)\frac{\partial \Phi}{\partial \eta}\right)=0, \tag{5}$$

which has the general solution,

$$\Phi=\sum_{m=0}^{\infty}[A_m P_m(\xi)+B_m Q_m(\xi)][A'_m P_m(\eta) + B'_m Q_m(\eta)]+\text{const}, \tag{6}$$

where $P_m(\cdot)$ and $Q_m(\cdot)$ are Legendre functions and associated Legendre functions of integer order m, respectively, and A_m, B_m, A'_m and B'_m are the constants of integration.

Since in the present case the range of interest includes $\eta=1$ (cf. Fig. 2) where $Q_m(1)=\infty$, to have a finite solution, we should take $B'_m=0$. Also in the present case it suffices to consider only the first term of Eq. (6) corresponding to $m=0$. We then obtain from Eq. (6)

$$\Phi=A''_0 P_0(\eta)[P_0(\xi)+B''_0 Q_0(\xi)]+\text{const}, \tag{7}$$

where $A''_0=A_0A'_0$, $B''_0=B_0/A_0$, $P_0(\eta)=P_0(\xi)=1$, and $Q_0(\xi)=(1/2)\ln[(1+\xi)/(1-\xi)]$.

Expression (7) then takes the form

$$\Phi=D\ln\left(\frac{1+\xi}{1-\xi}\right)+\text{const}, \tag{8}$$

where D is a constant determined by the circumstance that the free surface of the hyperboloid BCD at $\xi=\xi_0$ is kept at a potential of $\Phi_0=\varphi_0+$const. Then $D=\varphi_0/\ln[(1+\xi_0)/(1-\xi_0)]$, and

$$\Phi=\varphi_0\frac{\ln[(1+\xi)/(1-\xi)]}{\ln[(1+\xi_0)/(1-\xi_0)]}+\text{const}. \tag{9}$$

Note that a similar solution was found and used in Ref. 9.

Hyperboloid BCD is given by the expression,

$$\frac{z^2}{a_0^2}-\frac{\rho^2}{b_0^2}=1, \tag{10}$$

where

$$a_0^2=c^2\xi^2, \tag{11a}$$

$$b_0^2=c^2(1-\xi^2), \tag{11b}$$

and c is a constant.

The normal derivative of the electric potential at the surface of the liquid is given by

$$\left.\frac{\partial \Phi}{\partial n}\right|_{\xi=\xi_0}=\frac{1}{c}\left(\frac{1-\xi^2}{\eta^2-\xi^2}\right)^{1/2}\left.\frac{\partial \Phi}{\partial \xi}\right|_{\xi=\xi_0}, \tag{12}$$

which yields, using Eq. (9)

$$\left.\frac{\partial \Phi}{\partial n}\right|_{\xi=\xi_0}=\frac{2\varphi_0}{\ln[(1+\xi_0)/(1-\xi_0)]}\frac{1}{c[(\eta^2-\xi_0^2)(1-\xi_0^2)]^{1/2}}. \tag{13}$$

From Eq. (11a) it is seen that for the hyperboloid considered $c=a_0/\xi_0$.

Expression (13) characterizes the charge distribution over the free surface BCD with the largest charge per unit area near the tip, where $\eta=1$. The only nonzero stress of electrical origin acting on BCD is the normal stress,

$$\sigma_{nn}=\frac{1}{8\pi}\left.\left(\frac{\partial \Phi}{\partial n}\right)^2\right|_{\xi=\xi_0}, \tag{14}$$

which yields the stress distribution over the surface of the hyperboloid ξ_0,

$$\sigma_{nn}|_{\xi=\xi_0} = \frac{\varphi_0^2}{2\pi \ln^2[(1+\xi_0)/(1-\xi_0)]} \frac{1}{[(z^2/\xi_0^2 - a_0^2)(1-\xi_0^2)]}. \tag{15}$$

The z coordinates of points on the free surface are z.

It is emphasized that to arrive at Eq. (15) we also used Eq. (11a) and the first formula relating the cylindrical and the prolate spheroidal coordinates,

$$z = c\,\eta\xi, \tag{16a}$$

$$\rho = c[(1-\xi^2)(\eta^2-1)]^{1/2}. \tag{16b}$$

From Eq. (15) it follows that the stresses σ_{nn} at the tip of hyperboloid BCD at $z=a_0$ and $H \gg a_0$ are given by

$$\sigma_{nn}|_{z=a_0} = \sigma_{nn,\max} = \frac{\varphi_0^2}{2\pi \ln^2[(1+\xi_0)/(1-\xi_0)]} \left(\frac{\xi_0}{a_0}\right)^2 \frac{1}{(1-\xi_0^2)^2}, \tag{17a}$$

$$\sigma_{nn}|_{z=H} = \sigma_{nn,\min} = \frac{\varphi_0^2}{2\pi \ln^2[(1+\xi_0)/(1-\xi_0)]} \times \frac{1}{[(H^2/\xi_0^2 - a_0^2)(1-\xi_0^2)]}. \tag{17b}$$

It should be noted that the solutions obtained above for the electric field around hyperboloidal bodies are exact. However, for liquid bodies the shape of the free surface cannot, *a priori*, be expected to be a perfect hyperboloid and should be calculated separately.

Assuming a hyperboloidal shape as an approximation, its curvature is given by

$$K = \frac{(b_0 z/a_0)^2 - b_0^2 + (b_0^2 z/a_0^2)^2 + b_0^4/a_0^2}{[(b_0 z/a_0)^2 - b_0^2 + (b_0^2 z/a_0^2)]^{3/2}}. \tag{18}$$

Therefore the capillary pressures $p_\sigma = \sigma K$ at the tip and at a height H above the tip (see Fig. 2) is given by

$$p_\sigma|_{z=a_0} = \sigma \frac{2a_0}{b_0^2}, \tag{19a}$$

$$p_\sigma|_{z=H} = \sigma \frac{(b_0 H/a_0)^2 - b_0^2 + (b_0^2 H/a_0^2)^2 + b_0^4/a_0^2}{[(b_0 H/a_0)^2 - b_0^2 + (b_0^2 H/a_0^2)^2]^{3/2}}. \tag{19b}$$

Like in the first spheroidal approximation used by Taylor,[3] we approximate the force balance at the hyperboloidal surface by the expressions

$$\sigma K|_{z=a_0} - \Delta p = \sigma_{nn}|_{z=a_0}, \tag{20a}$$

$$\sigma K|_{z=H} - \Delta p = \sigma_{nn}|_{z=H}. \tag{20b}$$

Assuming that Δp, the difference between the pressure inside the surface and that outside it, is the same at the tip $z=a_0$ and "bottom" $z=H$, we obtain

$$\sigma_{nn}|_{z=a_0} - \sigma_{nn}|_{z=H} = \sigma K|_{z=a_0} - \sigma K|_{z=H}. \tag{21}$$

Substituting Eqs. (17) and (19) in Eq. (21), we find the dependence of φ_0 on the surface tension coefficient σ;

$$\frac{\varphi_0^2}{2\pi \ln^2[(1+\xi_0)/(1-\xi_0)]} \left[\left(\frac{\xi_0/a_0}{1-\xi_0^2} \right)^2 - \frac{1}{[(H/a_0)^2 - a_0^2](1-\xi_0^2)} \right] = \sigma \left(\frac{2a_0}{b_0^2} - \frac{(b_0 H/a_0)^2 - b_0^2 + (b_0^2 H/a_0^2)^2 + b_0^4/a_0^2}{[(b_0 H/a_0)^2 - b_0^2 + (b_0^2 H/a_0^2)^2]^{3/2}} \right). \tag{22}$$

Also from Eq. (11) we obtain

$$b_0^2 = a_0^2 \frac{(1-\xi_0^2)}{\xi_0^2}. \tag{23}$$

Substituting Eq. (23) in Eq. (22) and rendering Eq. (22) dimensionless, we rearrange it as follows:

$$\frac{\varphi_0^2}{\sigma a_0} = 2\pi \ln^2\left(\frac{1+\xi_0}{1-\xi_0}\right) \left(2\xi_0^2 - \frac{\xi_0 (1-\xi_0^2)^{1/2} [(\bar{H}^2+1)/\xi_0^2 - 2]}{[(\bar{H}/\xi_0)^2 - 1]^{3/2}} \right) \times \left(\frac{\xi_0^2}{1-\xi_0^2} - \frac{1}{[(\bar{H}/\xi_0)^2 - 1]} \right)^{-1}. \tag{24}$$

For a given $\bar{H} = H/a_0$ we obtain from expression (24) a dependence of $\varphi_0^2/\sigma a_0$ on ξ_0 for a stationary liquid body assumed to have a hyperboloidal shape. In the case of an "infinite" hyperboloid ($\bar{H} \gg 1$) with its tip at a distance a_0 from the equipotential surface $z=0$, expression (24) yields

$$\varphi_0 = (\sigma a_0)^{1/2} (4\pi)^{1/2} \ln\left(\frac{1+\xi_0}{1-\xi_0}\right) (1-\xi_0^2)^{1/2}, \tag{25}$$

which is analyzed in Sec. IV.

The temptation is to assign the equipotential surface $z=0$ to the ground plate at $z_1=0$. This assignment is ruled out, because a_0 would then be much larger than the droplet size. Then the electric field adjacent to the droplet [which is only a small detail of the practically uniform, capacitor-like field between the electrode and the ground; cf. Fig. 2(a)] would be grossly in error because this calculation does not account for the presence of the electrode at $z_1 = H_{ge}$. To eliminate this difficulty, we assume that the equipotential surface $z=0$ is situated very close to the droplet tip, at a distance a_0, which is yet to be determined. The electric field between the matching boundary [cf. Fig. 2(b)] and the free surface of the droplet was already determined, and was described above.

The electric field between the matching boundary and the ground plate at distances from the tip much larger than a_0 is practically unaffected by the droplet. Thus the electric field in the region between the ground plate and the matching boundary may be assumed to be that of a parallel-plate ca-

pacitor [cf. Fig. 2(a)]. The parallel-capacitor field and the field of the potential Φ found here in Sec. III [cf. Fig. 2(c)] are to be matched at $z=0$, which enables us to calculate a_0 [cf. Fig. 2(b)]. We can call the space between the surface $z=0$ and the hyperboloid the boundary layer, which is characterized by the scale a_0. The space below $z=0$ is then the ''outer field'' using a fluid-mechanical analogy. It is emphasized that this procedure is only a crude first approximation, since the normal derivatives of the potentials (the electric field intensities) are not automatically matched at $z=0$. A much better representation of the field and potential in the intermediate region could be achieved by matching asymptotic expansion or computer modeling. The region where the potential is not predicted with much precision is shown in gray in Fig. 2(b).

We now consider in detail matching of the approximate solutions for the electric potential. If z_1 is the coordinate directed from the ground plate (at $z_1=0$) toward the droplet, then the capacitor-like field is given by

$$\Phi=\frac{\Phi_0}{H_{ge}}z_1. \tag{26}$$

Here H_{ge} is the distance between the ground plate and an electrode attached to the droplet (at potential Φ_0).

Given that the droplet height in the z direction is H, that the borderline equipotential surface where $z=\xi=0$ is situated at $z_1=H_{ge}-H-a_0$, and matching the solutions for the potential, we find, from Eqs. (9) and (26), that the constant in Eq. (9) is

$$\text{const}=\frac{\Phi_0}{H_{ge}}(H_{ge}-H-a_0). \tag{27}$$

Thus Eqs. (9) and (27) yield

$$\Phi=\varphi_0\frac{\ln[(1+\xi)/(1-\xi)]}{\ln[(1+\xi_0)/(1-\xi_0)]}+\Phi_0\frac{(H_{ge}-H-a_0)}{H_{ge}}. \tag{28}$$

For the droplet surface at $\xi=\xi_0$, the potential is $\Phi=\Phi_0$, and thus from Eq. (28) we find

$$\varphi_0=\frac{\Phi_0}{H_{ge}}(H+a_0). \tag{29}$$

Combining Eq. (29) with Eq. (25), we obtain the equation for a_0,

$$(\sigma a_0)^{1/2}(4\pi)^{1/2}\ln\left(\frac{1+\xi_0}{1-\xi_0}\right)(1-\xi_0^2)^{1/2}=\frac{\Phi_0}{H_{ge}}(H+a_0), \tag{30}$$

which has two solutions. The solution relevant here reads

$$a_0=\frac{1}{2}\left(\frac{1}{\beta^2}-2H\right)-\left[\frac{1}{4}\left(\frac{1}{\beta^2}-2H\right)^2-H^2\right]^{1/2}, \tag{31a}$$

$$\beta=\frac{\Phi_0}{H_{ge}(4\pi\sigma)^{1/2}\ln[(1+\xi_0)/(1-\xi_0)](1-\xi_0^2)^{1/2}}, \tag{31b}$$

whereas the other one is not relevant, since it yields $a_0>H_{ge}$.

Expression (31a) permits calculation of a_0 for any given hyperboloidal droplet (given ξ_0 and H) at any given potential Φ_0. It should be noted that the calculated potential field will be accurate if the calculated value of a_0 is sufficiently small relative to H.

IV. FAILURE OF THE SELF-SIMILARITY ASSUMPTION FOR HYPERBOLOIDAL SOLUTIONS

The electric potential between the free surface of a hyperboloidal liquid body and the equipotential surface $z=0$ is given by Eq. (9) with φ_0 as per Eq. (25). To visualize the asymptotic behavior of Eq. (9), we should follow a straight line with a constant slope θ, while R tends toward infinity (see Fig. 1). Then using Eqs. (16) we find

$$R=(z^2+\rho^2)^{1/2}=c(\eta^2+\xi^2-1)^{1/2}. \tag{32}$$

Also

$$-\tan\theta=\frac{\rho}{z}=\frac{[(1-\xi^2)(\eta^2-1)]^{1/2}}{\eta\xi}, \tag{33}$$

which yields

$$\eta^2=\frac{1-\xi^2}{1-(\xi/\cos\theta)^2}. \tag{34}$$

Substituting the latter in Eq. (32), we find

$$R=c\,\frac{\xi}{-\cos\theta}\left(\frac{1-\xi^2}{1-(\xi/\cos\theta)^2}\right)^{1/2}. \tag{35}$$

It is seen that $R\to\infty$ as $\xi\to-\cos\theta$. Then we obtain from Eqs. (9) and (25) the potential Φ as $R\to\infty$ in the following form:

$$\Phi|_{R\to\infty}=(\sigma a_0)^{1/2}(4\pi)^{1/2}(1-\xi_0^2)^{1/2}\ln\left(\frac{1-\cos\theta}{1+\cos\theta}\right)+\text{const},\qquad \frac{\pi}{2}\leqslant\theta\leqslant\pi, \tag{36}$$

which shows that the asymptotic value, Φ, is finite. Φ does not tend toward infinity as the self-similarity of Sec. II implies. Also, in spite of the fact that $R\gg a_0$, the dependence on a_0 does not disappear from Eq. (36) in contrast with the self-similar behavior of Taylor's solution given by Eq. (3). We thus have here an example of a nonself-similar solution with a nonfading influence of the value of a_0, even when $R\gg a_0$. Details of the shape of the tip, at small distances, of the order of a_0, affect the solution for Φ at any $R\gg a_0$. In other words, the solution for the field about a hyperboloid depends on the value of a_0 everywhere, while the field surrounding the Taylor cone does not depend on a_0 at $R\gg a_0$. The field surrounding the hyperboloidal bodies is always affected by the value of a_0, even when R approaches ∞. This behavior is quite distinct from that of the boundary-layer theory cases of jets from a finite orifice and of plumes originating at a finite source, where the influence of the size of the orifice or source rapidly fades out. The calculated cone which is tangent to the critical hyperboloid just before a jet is ejected is definitely not the Taylor cone. Indeed, in Fig. 3 the dependence of $\varphi_0/(\sigma a_0)^{1/2}$ on ξ_0 according to Eq. (25) is shown. The maximal potential at which a stationary shape

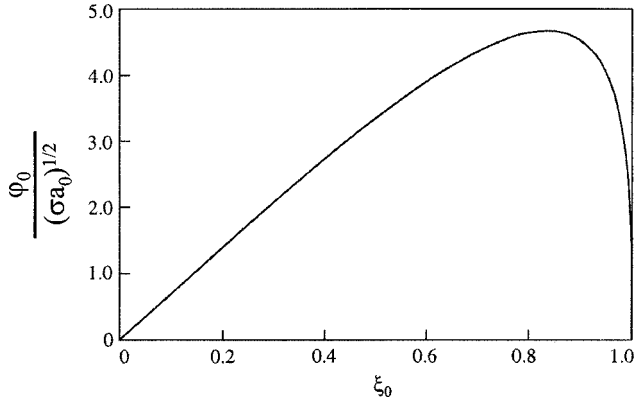

FIG. 3. Dependence of the shape parameter ξ_0 on the electric potential φ_0 of an infinite hyperboloid.

can exist corresponds to $\xi_{0*}=0.834$ and $\varphi_{0*}=4.699(\sigma a_0)^{1/2}$. The value ξ_{0*} corresponds to the critical hyperboloid. An envelope cone for any hyperboloid can be found using the derivative

$$\left.\frac{dz}{d\rho}\right|_{\rho\to\infty}=\frac{a_0}{b_0}, \tag{37}$$

which follows from Eq. (10).

For the critical hyperboloid, using Eq. (23), we find

$$\frac{a_0}{b_0}=\frac{\xi_{0*}}{(1-\xi_{0*}^2)^{1/2}}=1.51. \tag{38}$$

Therefore the half angle at the tip of the cone is given by (cf. Fig. 1)

$$\alpha_*=\frac{\pi}{2}-\arctan(1.51), \tag{39}$$

which yields $\alpha_*=33.5°$, which is significantly smaller than the angle for the Taylor cone, $\alpha_T=49.3°$. Note also that the Taylor cone is asymptotic to a different hyperboloid possessing a value of $\xi=\xi_{0T}$ which should be less than ξ_*. Indeed, similar to Eq. (38)

$$\frac{a_{0T}}{b_{0T}}=\frac{\xi_{0T}}{(1-\xi_{0T}^2)^{1/2}}=\tan\left(\frac{\pi}{2}-\alpha_T\right), \tag{40}$$

which yields $\xi_{0T}=\cos\alpha_T=0.65$. Comparing this value with that for the critical hyperboloid, $\xi_{0*}=0.834$, we see once more that the critical hyperboloid is much "sharper" than the one corresponding to the Taylor cone, since this sharpness increases with ξ.

The left part of the curve with a positive slope in Fig. 3 can be realized pointwise, since there higher potentials correspond to sharper hyperboloids. By contrast, the right-hand part represents still sharper hyperboloids for lower potentials, which cannot be reached in usual experiments with a stable fluid body. The latter means that the right-hand part corresponds to unstable solutions. It is also emphasized that the critical angle $\alpha_*=33.5°$ is much closer to the experimental values reported in Sec. VI than that of the Taylor cone.

The results of Secs. III and IV are equally relevant for inviscid, for Newtonian, or for viscoelastic liquids after the stress has relaxed. All these manifest stationary states with zero deviatoric stresses.

V. STATIONARY HYPERBOLOIDS OF ELASTIC LIQUIDS

In the hypothetical case of a purely elastic liquid without any stress relaxation, or for a viscoelastic liquid with relatively weak relaxation effects and stresses considered as stationary before the relaxation ceases, internal elastic forces should be included in the force balance alongside their electric and surface-tension counterparts. Such liquids are stretched when their electric potential is raised. We assume that before and after stretching the liquid body is hyperboloidal. The shape of a stationary free surface raised to a potential Φ_0 is described by Eq. (10) with the parameters a_0 and b_0, whereas the shape before stretching is also described by Eq. (10) but with the parameters a_{00} and b_{00}. The cylindrical coordinates corresponding to the stretched hyperboloid can be represented in the form

$$z=a_0\cosh\psi, \tag{41a}$$

$$\rho=b_0\sinh\psi, \tag{41b}$$

where ψ is a parameter.

Then the radius vector of a material point at the free surface $\mathbf{r}_0$ takes the form

$$\mathbf{r}_0=\mathbf{i}b_0\cos\theta\sinh\psi+\mathbf{j}b_0\sin\theta\sinh\psi+\mathbf{k}a_0\cosh\psi, \tag{42}$$

where $\mathbf{i}$, $\mathbf{j}$, and $\mathbf{k}$ are the unit vectors of the Cartesian coordinate system x, y, z, with x and y belonging to the same plane as ρ, and z being same as the corresponding cylindrical coordinate.

Similarly, the radius vector of the initial (stress-free) surface $\mathbf{r}_{00}$ is given by

$$\mathbf{r}_{00}=\mathbf{i}b_{00}\cos\theta\sinh\psi+\mathbf{j}b_{00}\sin\theta\sinh\psi+\mathbf{k}a_{00}\cosh\psi. \tag{43}$$

The deformation gradient tensor corresponding to the transformation of the reference vector $\mathbf{r}_{00}$ to that in the presence of the field, $\mathbf{r}_0$, is given by

$$\mathbf{F}=\frac{b_0}{b_{00}}(\mathbf{ii}+\mathbf{jj})+\frac{a_0}{a_{00}}\mathbf{kk}, \tag{44}$$

whereas the Green tensor $\mathbf{B}=\mathbf{F}\cdot\mathbf{F}^T$ is

$$\mathbf{B}=\left(\frac{b_0}{b_{00}}\right)^2(\mathbf{ii}+\mathbf{jj})+\left(\frac{a_0}{a_{00}}\right)^2\mathbf{kk}. \tag{45}$$

We assume the neo-Hookean constitutive model for stress deviator tensor[12]

$$\boldsymbol{\tau}=2G_0\mathbf{B}, \tag{46}$$

where G_0 is the modulus of elasticity.

The force balances, Eqs. (20), are modified to account for the elastic stresses according to Eqs. (45) and (46) and take the form

$$\sigma K|_{z=a_0} - \Delta p = \sigma_{nn}|_{z=a_0} - 2G_0\left(\frac{a_0}{a_{00}}\right)^2, \tag{47a}$$

$$\sigma K|_{z=H} - \Delta p = \sigma_{nn}|_{z=H} - 2G_0\left(\frac{b_0}{b_{00}}\right)^2, \tag{47b}$$

which results in

$$\sigma_{nn}|_{z=a_0} - \sigma_{nn}|_{z=H} = \sigma K|_{z=a_0} - \sigma K|_{z=H} + 2G_0\left[\left(\frac{a_0}{a_{00}}\right)^2 - \left(\frac{b_0}{b_{00}}\right)^2\right]. \tag{48}$$

The latter generalizes Eq. (21) for the case of an elastic liquid.

Using Eqs. (11), we obtain

$$\left(\frac{a_0}{a_{00}}\right)^2 - \left(\frac{b_0}{b_{00}}\right)^2 = \left(\frac{\xi_0}{\xi_{00}}\right)^2\left(1 - \frac{\xi_{00}^2(1-\xi_0^2)}{\xi_0^2(1-\xi_{00}^2)}\right), \tag{49}$$

where ξ_{00} and ξ_0 are the values of the coordinate ξ corresponding to the reference (stress free) and actual configuration of the free surface.

Substituting Eqs. (17), (19), and (49) in Eq. (48), we obtain

$$\frac{\varphi_0^2}{\sigma a_0} = \left[2\pi \ln^2\left(\frac{1+\xi_0}{1-\xi_0}\right)\left(2\xi_0^2 - \frac{\xi_0(1-\xi_0^2)^{1/2}[(\bar{H}^2+1)/\xi_0^2 - 2]}{[(\bar{H}/\xi_0)^2 - 1]^{3/2}}\right) + \frac{G_0 a_0}{\sigma} \times 4\pi(1-\xi_0^2)\ln^2[(1+\xi_0)/(1-\xi_0)](\xi_0/\xi_{00})^2 \times \left(1 - \frac{(\xi_{00}/\xi_0)^2(1-\xi_0^2)}{1-\xi_{00}^2}\right)\right] \times \left(\frac{\xi_0^2}{(1-\xi_0^2)} - \frac{1}{[(\bar{H}/\xi_0)^2 - 1]}\right)^{-1}, \tag{50}$$

which generalizes Eq. (24) for the case of an elastic liquid.

Estimating $G_0 \sim \mu_0/\theta$, where μ_0 is the zero-shear viscosity and θ is the relaxation time, and taking $\mu_0 = 10^4$ g/(cm s), $\theta = 10^{-1}$ s, $a_0 = 10^{-3}$ cm, and $\sigma = 70$ g/s^2, we obtain $G_0 a_0/\sigma \sim 1$. Figure 4 was calculated using Eq. (50) with $\bar{H} = 3$, $G_0 a_0/\sigma = 1$, and $\xi_{00} = 0.3$. The results show that the critical value of ξ_0 is $\xi_{0*} = 0.693$, which means that the elastic forces reduced the sharpness of the critical hyperboloid. The half angle of the cone which is tangent to the fluid body is increased to $\alpha_* = 47.83°$, which is still less than that for the Taylor cone. The elastic forces certainly have a stabilizing effect and they resist (along with the surface tension forces) the disrupting electric forces.

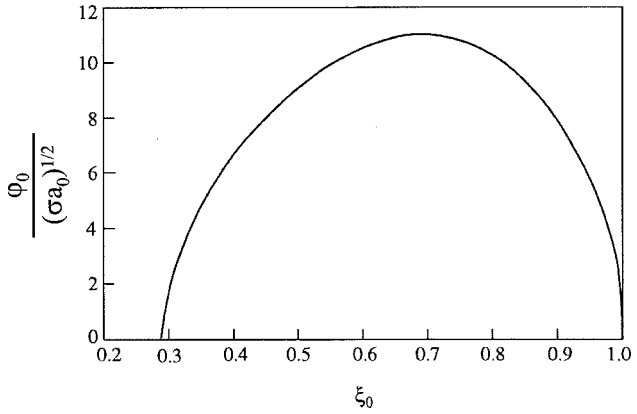

FIG. 4. Dependence of the shape parameter ξ_0 on the electric potential φ_0 of an elastic hyperboloid.

VI. EXPERIMENTAL RESULTS AND COMPARISON WITH THE THEORY

Two experiments, using sessile and pendant droplets, were performed for comparison with the theory. These experiments continue activities on electrospinning of nanofibers already reported.[13,14]

In the sessile drop experiment (Fig. 5) a droplet was created at the tip of an inverted pipette by forcing the liquid through the pipette with a syringe pump. The liquid used was an aqueous solution of polyethylene oxide with a molecular weight of 400 000, and a weight concentration of 6%. Fluid properties of such solutions including shear and elongational viscosity, surface tension, and conductivity/resistivity are published elsewhere.[13–15] Their evaporation rate can be described using the standard dependence of saturation vapor concentration on temperature.[14] For droplet sizes of the order of 0.1 cm, the evaporation process lasts not less than 600 s.[16] This is much more than the time required to reach steady state and make measurements (of the order of 1 s). Therefore evaporation effects when the photographs were taken are negligible. All the experiments were done at room tempera-

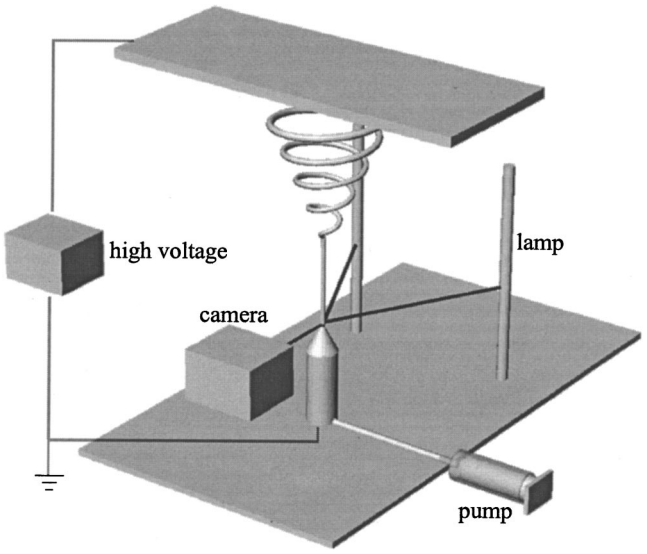

FIG. 5. Sessile drop experiment.

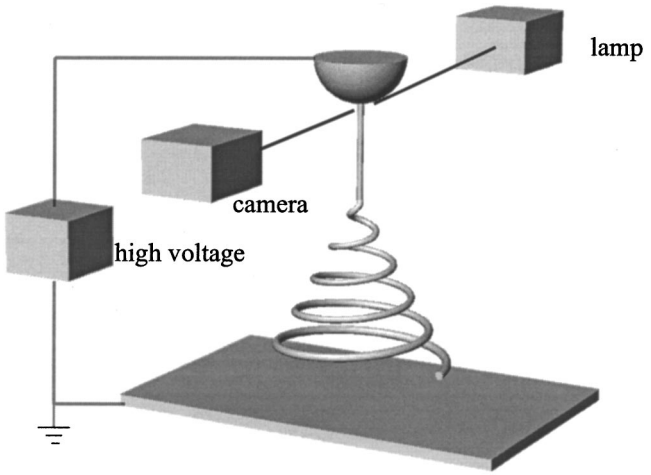

FIG. 6. Pendant drop experiment.

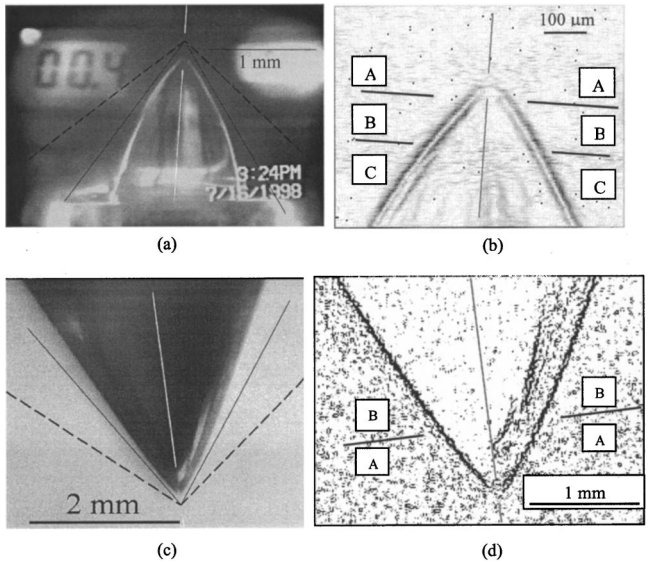

FIG. 7. (a) Videograph of the critical droplet shape observed for a sessile droplet. The bottom of the drop was constrained to the inner diameter of the pipette on which it sat. The drop is symmetrical about the white line. The symmetry axis is not exactly vertical due to camera tilt, the tilt of the pipette, and the tilt of the electric field direction. The half angles predicted in this article are indicated by the solid lines. The half angle associated with the Taylor cone is indicated by the dashed lines. This image was not enhanced or cropped. The outlines of the pipette can be seen at the bottom, and information on the experimental parameters is visible in the background. (b) Part of the image in (a), processed with Scion Image "Find Edges" (http://www.scioncorp.com/). No useful data about the location of the edge were found in region A. Lines tangent to the boundary segments in region B indicate a half angle of 37.5°. Lines tangent to the boundary segments in region C indicate a half angle of 30.5°. The lower parts of the boundary were not used because they were constrained by the pipette. (c) Critical droplet shape observed for a pendant drop. (d) Part of the image in (c). The enlarged droplet tip from (c), processed with Scion Image "Find Edges." Lines tangent to the boundary segments in region A indicate a half angle of 31°. Lines tangent to the boundary segments in region B indicate a half angle of 26°.

ture. Elevated temperatures were not studied. Droplet configurations are quite reproducible for a given capillary size, which was not varied in the present experiments. The effect of pH was not studied in detail. Addition of sodium chloride to the solution was discussed in Ref. 15. The electrode material, usually copper, had no important effect on the ionic conductivity of the solutions.[13–15]

The electric potential was applied between the droplet and a flat metal collector plate held above the droplet. The droplet was kept at ground potential for convenience. The potential difference was increased in steps of about 200 V, each step a few seconds long, until a jet formed at the tip of the droplet. Images of the droplet were made with a video camera. The shape of the droplet during the step that preceded the formation of the jet was called the critical shape. Two linear lamps were mounted vertically, behind and on either side of the droplet. The shape and diameter of the sessile droplet were demarcated by reflection of the lights, seen as white lines on the image recorded by the video camera. Diffuse back lighting was used for the pendant drop (Fig. 6).

The drops were photographed at a rate of 30 frames per second. The observed shape of the droplet is compared with calculated shapes in Fig. 7(a).

In the pendant droplet experiment (Fig. 6) the polymer solution was placed on a spoon with a 1 mm hole in its bowl. The potential was applied between the drop and a flat plate. The experimental result is shown in Fig. 7(b).

The sessile droplet, which was attracted toward a flat electrode at a distance $H_{ge}=13$ cm, became critical at the potential $\Phi_0=19.34\,\mathrm{kV}=64.47\,(\mathrm{g\,cm})^{1/2}/\mathrm{s}$. The drop had a height of $H=0.128$ cm. When Φ_0 was slightly increased by a step of about 200 V, a jet emerged from the top of the droplet. Using these data, as well as $\xi_0=\xi_{0*}=0.834$ (cf. Sec. IV), and taking $\sigma=70\,\mathrm{g/s^2}$, the value of a_0 was found from Eq. (31) to be $a_0=0.000\,26$ cm. Since the value of a_0 is much smaller than H, the hyperboloidal approximation, not accounting for perturbations due to the electrode, is self-consistent and satisfactory (see the earlier discussion near the end of Sec. III).

The pendant droplet became critical at the potential $\Phi_0=19.5\,\mathrm{kV}=65.6\,(\mathrm{g\,cm})^{1/2}/\mathrm{s}$ at $H_{ge}=17.3$ cm [see Fig. 7(b)]. The height of the droplet was $H=0.30$ cm. The value of a_0 was found to be 0.000 21 cm, which is also sufficiently small relative to H. The corresponding value of the potential difference between the droplet and the equipotential surface at the matching boundary is $\varphi_{0*}=4.699(\sigma a_0)^{1/2}=0.57\,(\mathrm{g\,cm})^{1/2}/\mathrm{s}=171$ V.

The hyperboloids calculated using Eqs. (10) and (25) approach the conical asymptotes with a half angle of $\alpha_*=33.5°$, which are shown by the solid lines in Fig. 7. Cones with a half angle of $\alpha_T=49.3°$, which is characteristic of the Taylor cone, are shown in Fig. 7 by dashed lines. The half angle at the tip, in the photographs of Figs. 7(a) and 7(b) in region C, where the influence of the pipette is small, is 30.5°. Even closer to the tip in region B is an observed half angle is 37.5°. Both these angles are closer to the hyperboloidal solution (33.5°) than to the Taylor solution (49.3°). Calculation predicts that the hyperboloid approaches within 5 μm of the intersection of the asymptotes, but there is not enough resolution in the images that this can be seen. Half angles were measured, as shown in Fig. 7. For the sessile drop the measured half angle near the tip in region B was 37.5° and in region C it was 30.5°. For the pendant drop the

measured half angle near the tip in region A was 31° and in region B it was 26°. All these angles are closer to the hyperboloidal solution than to the Taylor cone.

Note also that the electrode used in the experiments was submerged in the liquid inside the pipette so the influence of the actual electrode on the shape of the droplet is minimal. The lower part of the droplet, shown in Fig. 7(a), is also affected mechanically by the pipette wall, which restricts the diameter of the base of the droplet. That is the reason why the free surface deviates from the predicted solid line in Fig. 7(a) near the bottom.

It should be mentioned that in Ref. 17 it was stated that, according to experimental data, a stable cone can be obtained for a range of angles, but typically the half angle was close to 45°. Both Taylor[3] and Michelson[17] worked with low molecular weight liquids, which are prone to perturbations and atomization. These perturbations might lead to premature jetting before a true critical shape can be achieved. This can explain the larger (and varying) values of α recorded in the experiments of Refs. 3 and 17.

In Ref. 18 critical configurations of liquid droplets affected by the electric field in a parallel capacitor were calculated numerically using the boundary element method. One of the arrangements considered, the initially hemispherical droplet supported by an electrode, is close to the experimental situation in the present work. The numerical predictions for this case (Fig. 42 of Ref. 18) showed that the angle of the cone fit to the calculated shape is less than or about 40°, which is closer to the critical angle $\alpha^*=33.5°$ predicted in the present work than to $\alpha_T=49.3°$.

The numerically predicted value of the half angle of the calculated shape, which is significantly less than 49.3°, may be an indication of failure of the self-similarity assumption, similar to what was discussed in Sec. IV of the present work. However, due to inaccuracies intrinsic in numerical methods in cases in which a singularity is formed, a definite statement cannot be made. According to Ref. 19, in which both boundary and finite element calculations related to the present problem were characterized, ''all the numerical studies either assume a rounded end and/or cannot resolve the structure in the neighborhood of a nearly pointed end.'' As usual, close to singularities, insight can be gained by approximate models, for example, the slender body approximation,[19–21] or the hyperboloidal approximation of the present work.

A recent attempt[22] to simulate numerically dynamics of Taylor cone formation revealed the following. In one of the two cases considered the free surface developed a protrusion which did not approach a conelike shape before the calculations were stopped. In the second case a cone-like structure with a half angle of about 50.5° was achieved after the calculations were started from a very large initial perturbation. It should be mentioned that the generatrix of the initial perturbation was assumed to be given by the Gaussian function, and liquid was assumed to be at rest. These assumptions are arbitrary and non-self-consistent. Also, the assumed initial shape was far from a spherical droplet relevant within the context of polymeric fluids. Moreover, the value assumed for the electric field was chosen arbitrarily and could have exceeded the critical electric field for a stationary Taylor cone. All this makes the results inconclusive and shows that the dynamic theory of Taylor cone formation deserves further effort.

It is emphasized that the present work, following that of Taylor,[3] assumes the liquid in the droplet to be a perfect conductor. In a number of works cases where liquid in the drop is an insulator were considered.[19,21,23] Two self-similar conical solutions with half angles of $0°\leqslant\alpha^*\leqslant 49.3°$ exist when the ratio of the dielectric constants is in the range of $17.59\leqslant\epsilon_d/\epsilon_s\leqslant\infty$, where ϵ_d corresponds to the droplet, and ϵ_s corresponds to a surrounding fluid (the ratio $\epsilon_d/\epsilon_s=\infty$ corresponds to the fully conductive droplet). For $\epsilon_d/\epsilon_s<17.59$ equilibrium conical solutions do not exist. Deviation of the experimental half angles to values significantly below 49.3° can, in principle, be attributed to one of the two solutions for the range of ϵ_d/ϵ_s where two solutions exist. The choice between these solutions based on the stability arguments leads to the rather puzzling outcome that the Taylor cone branch is unstable, and that very small half angles should be taken (in contradiction to experiment).[19,21] However, the assumption that liquids could be considered as insulators actually holds only on time scales shorter than the charge relaxation times. The latter are of the order of 10^{-10}–10^{-5} s according to the estimates in Ref. 23. Since in our experiments the residence time of a liquid in the cone is much longer than the charge relaxation time, conductivity effects should be added to the dielectric effects.[23] In insulating dielectric liquids, due to nonzero electric shear stress at the cone surface, flow is inevitable inside the droplet.[23] In the experiments of the present work such a flow was not seen. The absence of such flow is consistent with the fact that the behavior of the polymer solutions used could be closely approximated by that of a perfectly conductive liquid, as was assumed.

It is of interest to estimate the radius of curvature r at the tip at the potential which corresponds to the onset of instability. From Eq. (19a), we have $r=b_0^2/2a_0$. Using Eq. (23) we find

$$r=a_0\frac{(1-\xi_0^2)}{2\xi_0^2}. \tag{51}$$

Substituting here $\xi_0=0.834$ and $a_0=0.000\,26$ cm, which are the values found above, we find $r=5.69\times10^{-5}$ cm, which is near the wavelength of light and is too small to be seen in an ordinary photograph. Dimensions of polymer molecules, such as the radius of gyration in the solution, are typically around 10 nm(10^{-6} cm), and therefore can be neglected.

In group of works related to the development of pure liquid alloy ion sources (LAIS)[24–26] several additional physical processes, which may be relevant within the context of Taylor cone formation, were revealed. The most important of them is field evaporation of metal ions from the tip of the cone leading to emergence of ion emission currents and space charge. These phenomena are totally irrelevant in the present context for the following reasons. According to Refs. 24–26 field evaporation is impossible unless a jet-like protrusion is formed on top of the Taylor cone. The characteristic radius of curvature of the protruding tip should be of the order of 1–1.5 nm, and the corresponding field strength of

the order of 1.5×10^5 kV/cm. These conditions could never be realized in the present experiments. In the present case, unlike in LAIS, the huge fields needed for field evaporation could not even be approached. Moreover, the apex temperatures corresponding to field evaporation and the accompanying effects are of the order of 600–1000 °C according to Ref. 25. Such temperatures would produce drastic chemical changes in a polymer solution.

In the course of the present work space charge and electrical currents in the air were occasionally measured. It was shown that the occurrence of these phenomena was always a consequence of corona discharge, and could always be reduced to a very low level. All the above taken together allows us to conclude that field evaporation and ion current effects on the half angle of the observed cones can be totally disregarded.

For low viscosity liquids, as already mentioned, tiny droplets can easily be emitted from the cone tip. Sometimes droplet emission begins at α_* close to 45°,[17] sometimes close to 49°.[27] It should be emphasized that single tiny protrusions, jets, and droplets of submicron size at the top of the Taylor cone are invisible in ordinary photographs. It is difficult to judge when the jet emerges since the cone tip may oscillate as each droplet separates. At higher voltage, atomization of the cone tip can lead to significant space charge from the electrically charged droplets emitted. In Ref. 27 it was shown that the backward electric effect of the charged droplets on the tip of the cone leads to reduction of its half angle to a range of $32°<\alpha_*<46°$. For the highly viscoelastic liquids we are dealing with in the present work, atomization is virtually impossible. Breakup of tiny polymer jets, threads, and filaments is always prevented by viscoelastic effects and the huge elongational viscosity associated with them.[13,14,28,29] Therefore it is highly improbable that the reduced values of the half angle α_* found in the present experiments can be attributed to a space charge effect similar to that in Ref. 27.

When the critical potential for static cone formation is exceeded, jetting begins from the tip. In the relevant case of polymer solutions the jets are stable to capillary perturbations, but are subject to bending instability,[13,14] which is usually observed in the electrospinning process. On the other hand, in the case of low viscosity liquids or removal of the charge,[15] the jets are subject to capillary instability,[3] which sometimes leads to an almost immediate disappearance of the jet.[27] Sometimes, however, in the case of bending or capillary instability a visible, almost straight section of a jet exists, where the growing perturbations are still very small. Therefore it is of interest to describe the jet profile corresponding to the almost straight section. This is typically done within the framework of the quasi one-dimensional equations of dynamics of free liquid jets.[13,28,30–33] In Refs. 32 and 33 such a solution for the jet was also matched with a conical semi-infinite meniscus using the method of matched asymptotic expansions. As a basic approximation for the droplet shape, a Taylor cone of $\alpha_T=49.3°$ was chosen. In light of the present results a similar calculation is worth doing for an almost conical hyperboloidal droplet with $\alpha_*=33.5°$.

VII. SUMMARY

The hyperboloidal approximation employed permits prediction of the stationary critical shapes of drops of inviscid, Newtonian, viscoelastic, and purely elastic fluids. It was shown, both theoretically and experimentally, that, as a liquid surface develops a critical shape, its configuration approaches the shape of a cone with a half angle of 33.5°, rather than a Taylor cone of 49.3°.

The critical half angle does not depend on fluid properties for Newtonian fluids, since an increase in surface tension is always accompanied by an increase in the critical electric field. However, the sharpness of the critical hyperboloid depends on elastic forces and surface tension in elastic fluids or in unrelaxed viscoelastic fluids.

ACKNOWLEDGMENTS

One of the authors (A.L.Y.) was partially supported by the GIF-German–Israeli Foundation for Scientific Research and Development, Research Grant No. I-536-097.14/97, and by the Israel Science Foundation, and the Israel Academy of Sciences, Grant No. 287/00-1. Experimental work was partially supported by the National Science Foundation under Grant Nos. CTS-9900949 and DMI-9813098, by Army Research Office MURI Grant No. 95-0950-01-06, and by the U.S. Army Soldier and Biological Systems Command. The help of Dr. Dan Galehouse with the design of experiments is greatly appreciated.

[1] Lord Rayleigh, Philos. Mag. **14**, 184 (1882).
[2] J. Zeleny, Proc. Cambridge Philos. Soc. **18**, 71 (1915).
[3] G. I. Taylor, Proc. R. Soc. London, Ser. A **258**, 383 (1964).
[4] H. Schlichting, *Boundary Layer Theory*, 7th ed. (McGraw–Hill, New York, 1979).
[5] Ya. B. Zel'dovich, JETP **7**, 1463 (1937); *Selected Works of Ya. B. Zel'dovich*, Vol. 1 Chemical Physics and Hydrodynamics (Princeton University Press, Princeton, NJ, 1992).
[6] K. E. Dzhaugashtin and A. L. Yarin, J. Eng. Phys. **32**, 666 (1977).
[7] A. L. Yarin and D. A. Weiss, J. Fluid Mech. **283**, 141 (1995).
[8] A. F. Spivak and Y. A. Dzenis, J. Appl. Mech. **66**, 1026 (1999).
[9] C. F. Eyring, S. S. Mackeown, and R. A. Millikan, Phys. Rev. **31**, 900 (1928).
[10] D. R. Kingham and L. W. Swanson, Appl. Phys. A: Solids Surf. **34**, 123 (1984).
[11] W. R. Smythe, *Static and Dynamic Electricity*, 3rd ed. (McGraw-Hill, New York, 1968).
[12] L. R. Treloar, *Physics of Rubber Elasticity* (Oxford University Press, Oxford, 1958).
[13] D. H. Reneker, A. L. Yarin, H. Fong, and S. Koombhongse, J. Appl. Phys. **87**, 4531 (2000).
[14] A. L. Yarin, S. Koombhongse, and D. H. Reneker, J. Appl. Phys. **89**, 3018 (2001).
[15] H. Fong, I. Chun, and D. H. Reneker, Polymer **40**, 4585 (1999).
[16] A. L. Yarin, G. Brenn, O. Kastner, D. Rensink, and C. Tropea, J. Fluid Mech. **399**, 151 (1999).
[17] D. Michelson, *Electrostatic Atomization* (Hilger, Bristol, 1990), p. 93.
[18] M. T. Harris and O. A. Basaran, J. Colloid Interface Sci. **161**, 389 (1993).
[19] H. A. Stone, J. R. Lister, and M. P. Brenner, Proc. R. Soc. London, Ser. A **455**, 329 (1999).
[20] J. D. Sherwood, J. Phys. A **24**, 4047 (1991).
[21] H. Li, T. C. Halsey, and A. Lobkovsky, Europhys. Lett. **27**, 575 (1994).
[22] V. G. Suvorov and E. A. Litvinov, J. Phys. D **33**, 1245 (2000).
[23] A. Ramos and A. Castellanos, Phys. Lett. A **184**, 268 (1994).
[24] R. G. Forbes and G. L. R. Mair, J. Phys. D **15**, L153 (1982).

[25] P. D. Prewett, G. L. R. Mair, and S. P. Thompson, J. Phys. D **15**, 1339 (1982).
[26] W. Driesel, Ch. Dietzsch, and R. Muhle, J. Vac. Sci. Technol. B **14**, 3367 (1996).
[27] J. Fernandez de la Mora, J. Fluid Mech. **243**, 561 (1992).
[28] A. L. Yarin, *Free Liquid Jets and Films: Hydrodynamics and Rheology* (Longman, Harlow, and Wiley, New York, 1993).
[29] M. Stelter, G. Brenn, A. L. Yarin, R. P. Singh, and F. Durst, J. Rheol. **44**, 595 (2000).
[30] A. M. Ganan-Calvo, J. Fluid Mech. **335**, 165 (1997).
[31] A. M. Ganan-Calvo, J. Aerosol Sci. **30**, 863 (1999).
[32] L. T. Cherney, J. Fluid Mech. **378**, 167 (1999).
[33] L. T. Cherney, J. Aerosol Sci. **30**, 851 (1999).